Effects of the Ethylene–Propylene–Diene Monomer Microstructural Parameters and Interfacial Compatibilizer Upon the EPDM/Montmorillonite Nanocomposites Microstructure: Rheology/Permeability Correlation

Y. Mohammadpour, A. A. Katbab

Department of Polymer Engineering, Amirkabir University of Technology, Tehran, Iran

Received 24 February 2007; accepted 5 June 2007
DOI 10.1002/app.26978
Published online 7 September 2007 in Wiley InterScience (www.interscience.wiley.com).

ABSTRACT: Attempts have been made to investigate the effects of ethylene–propylene–diene monomer (EPDM) rubber structural parameters on the developed microstructure, mechanical properties, rheology, and oxygen gas permeability of EPDM/organically modified montmorillonite (O-MMT) nanocomposite samples prepared via melt mixing. Maleic anhydride grafted EPDM (EPDM-*g*-MAH) has been employed as an interfacial compatibilizer. The influence of the EPDM melt viscosity and chain linearity on the extent of exfoliation of the clay nanolayers has been evaluated through the calculation of the nanolayer aspect ratio (length/thickness) with the Halpin–Tsai model. The results are consistent with the X-ray diffraction patterns of the samples. The flocculation of the clay nanolayers has been found to be more probable when O-MMT is mixed with highly branched, low-molecular-weight EPDM. More exfoliation occurs when EPDM rubber with a high molecular weight but low branching is used. This has been confirmed by more nonlinear melt rheology behavior and broadening of the retardation time spectra. Maleated EPDM has been shown to be effective in enhancing the molecular intercalation of the clay nanolayers and the prevention of flocculation in both low-molecular-weight and high-molecular-weight EPDM matrices. Dynamic melt rheology measurements have revealed nonterminal behavior within the low-frequency range by interfacially compatibilized molten samples with an EPDM-*g*-MAH/clay ratio of 3, regardless of the matrix molecular weight and chain linearity. © 2007 Wiley Periodicals, Inc. J Appl Polym Sci 106: 4209–4218, 2007

Key words: compatibilization; matrix; microstructure; nanocomposites; structure-property relations

INTRODUCTION

Polymer nanocomposites (organic/inorganic hybrids) have attracted great academic and industrial attraction during the last decades[1–20] because of the outstanding properties exhibited by those materials at low nanofiller contents. The unexpected beneficial behavior of nanocomposites is mainly attributed to the high filler/matrix and filler/filler interactions resulting from the huge surface area of well-dispersed nanoparticles. The extent of the interactions is controlled by the shape and aspect ratio (length to thickness) of the nanoparticles; therefore, all properties of nanocomposite polymer materials are influenced by the interface and interphase characterization. Layered silicates of natural bentonite and montmorillonite of synthetic origin possess a layer thickness of approximately 1 nm, whereas the lateral dimension may reach several micrometers. Nowadays, considerable research interest is focused on nanocomposites prepared by the incorporation of layered silicates into various polymeric matrices.[1–8] However, to achieve efficient property improvements, the gallery spaces between the layers should be made accessible for the polymer molecules. This occurs through the replacement of the alkali cations with a bulky cationic organic surfactant, which not only makes the silicate nanoparticles more hydrophilic and more compatible with polymer matrices but also increases the interlayer distance between the clay silicate layers. The resulting organophilic clay can then be intercalated by polymer chains in either a solution or molten state subjected to a shear stress field.[1,2] Polymer/layered silicate nanocomposites exhibited superior mechanical properties,[1–6] reduced gas permeability,[20] improved solvent resistance,[1] and enhanced thermal resistance. Generally, two idealized types of microstructures are expected when a polymer matrix is interacted with organomodified clay particles: intercalated and exfoliated. In an intercalated structure, polymer chains reside between the silicate layers, whereas in an exfoliated hybrid, the silicate nanolayers are randomly dispersed throughout the polymer matrix. Polymer/

Correspondence to: A. A. Katbab (katbab@aut.ac.ir).

Journal of Applied Polymer Science, Vol. 106, 4209–4218 (2007)

TABLE I
Characteristics of the EPDM Rubbers

EPDM grade	ML1+4 at 125°C	Ethylene (%)	Linearity	Supplier	Diene type
Keltan 2340A	25	54	Controlled long-chain branching	DSM (Holland)	ENB
Keltan 8340A	85	54	Controlled long-chain branching	DSM (Holland)	ENB
Vistalon 7500	85	55	Linear chain with a high-molecular-weight fraction	Exxon Mobil	ENB

ENB, ethylidene-norbornene.

layered silicate nanocomposites are synthesized by different methods, such as *in situ* polymerization, a solution method, and melt intercalation.[5–7,14,15] However, industry prefers to prepare olefinic polymers—thermoplastic resins, elastomers, or thermoplastic elastomers—by melt-compounding techniques. In most cases, an interfacial compatibilizer is essential for enhancing the interaction between the polymer and silicate nanofillers.

Rubber/clay nanocomposites have drawn great attention in recent years.[5–12] Okada et al.[8] reported that only 10 phr organoclay could enhance the tensile strength of acrylonitrile–butadiene rubber to make it comparable to that of acrylonitrile–butadiene rubber loaded with 40 phr carbon black. The gas permeability of styrene–butadiene rubber was reduced significantly by the inclusion of clay nanolayers into this elastomer.[12] EPDM rubber is a widely used engineering elastomer with outstanding resistance toward ozone degradation combined with high thermal stability, and so EPDM/clay nanocomposite materials have been found to be valuable. However, this elastomer does not have any polar groups in the backbone of its chain; therefore, a high interaction between the EPDM chains and clay layers is hardly achieved unless a suitable compatibilizer is used. Moreover, the EPDM structural parameters are expected to play a critical role in the development of the final nanocomposite morphology.

In this work, the effects of the EPDM molecular weight and its structural branching on the type of nanocomposite microstructure formed during a shear melt-mixing process have been investigated. The degree of effectiveness of maleic anhydride grafted (EPDM-*g*-MAH) as an interfacial compatibilizer with respect to the extent of intercalation or exfoliation of the nanoclay particles has also been studied and correlated with the oxygen gas permeability and mechanical properties. The developed microstructure has also been examined by dynamic melt rheology measurements.

EXPERIMENTAL

Material

Three EPDM rubber grades with different structural characteristics were used, as shown in Table I. EPDM-*g*-MAH (OPTIM P-635), with a graft percentage of 0.4, was supplied by Pluss Polymers Pvt., Ltd. (New Delhi, India). The organoclay was montmorillonite intercalated by dimethyl dehydrogenated tallow ammonium, with the commercial name of Dellite 67G, and it was provided by Laviosa Chemica Mineraria S.p.A. (Livorno, Italy). Analytical-grade hexadecane (Merck, Whitehouse Station, NJ) was used as a solvent. All other chemicals, including the curing agent, were used as received. The formula of the curing system added to the EPDM compounds is presented in Table II.

Preparation of the EPDM/clay nanocomposite samples

Different EPDM/organoclay and EPDM/EPDM-*g*-MAH/organoclay composite samples were prepared by a melt-compounding method with the compositions given in Table III. EPDM-*g*-MAH was first melt-hybridized with the organoclay in a Banbury-type internal mixer (HBI System 90, Haake Buchler, Sattle Brook, NJ) at 180°C and a rotor speed of 60 rpm. EPDM-*g*-MAH was first fed into the mixer, and the organoclay was incorporated after 1 min; mixing was continued until the mixing torque was stabilized. The prepared master batch was removed and mixed with the desired EPDM rubber in a laboratory-size two-roll mill (Farrel Bridge, London, UK) with a mill temperature of 60°C for 10 min. The curing ingredients were then added, and compounding was continued for 3 min.

The compounds were sheeted and vulcanized at 165°C in a compression molding press with a 2.5–

TABLE II
Vulcanizing Systems

Ingredient	phr
EPDM + EPDM-*g*-MAH	100
ZnO	5
Stearic acid	1.5
MBT	0.9
CZ	0.7
Sulfur	1.5
O-MMT	0 or 5.8

MBT, mercaptomercothiazole.

TABLE III
Sample Compositions

Compatibilizer (%)	Organoclay (%)	EPDM type	Code
0	0	Keltan 2340A	200
0	0	Keltan 8340A	800
0	0	Vistalon 7500	700
0	5	Keltan 2340A	250
0	5	Vistalon 7500	750
0	5	Keltan 8340A	850
5	5	Keltan 2340A	255
5	5	Vistalon 7500	755
5	5	Keltan 8340A	855
15	5	Keltan 2340A	2515
15	5	Vistalon 7500	7515
15	5	Keltan 8340A	8515

3-mm mold. The curing times for different compounds were determined on the basis of the optimum cure (the time to achieve 90% of the cure), which was read from the curing rheograph obtained for each compound with a Monsanto model 100S rubber rheometer (Winnipeg, Canada).

Characterization

X-ray diffraction (XRD) spectra were collected in a reflection mode with Ni-filtered Cu Kα radiation (λ = 0.154056 nm) at a generator voltage of 30 kV and a generator current of 30 mA with a Philips Expert diffractometer (Hamburg, Germany). Samples were scanned in a step mode in the range of 1.5–10°.

The tensile test and tensile behavior of the samples was evaluated with a Monsanto model T500 tensile tester at 25°C and a crosshead speed of 500 mm/min according to ASTM Standard D 412. Two sheets of each composition were prepared, and three samples from each sheet were examined. The most frequent test result was considered.

The melt rheology of the samples was determined with a Paar Physica US200 rheometric mechanical spectrometer (Graz, Australia) with a set of 25-mm-diameter parallel plates at 180°C. The strain amplitude was selected within the linear viscoelastic region (1%).

Thermogravimetric analysis (TGA) was performed to evaluate the thermal behavior of the samples. For this purpose, a DuPont model 951 thermogravimetric analyzer (Austin, TX) was used, and thermograms were obtained under air and with a scanning rate of 10°C/min according to ASTM Standard E 2105.

The solvent resistance was determined by the immersion of a weighted predried sample in hexadecane at room temperature. The weight increase was measured 1 min after its removal from the solvent.

The oxygen gas transmission rates of the samples were measured at 20°C and 90% relative humidity with GDP-C 150 (Germany), which is based on ASTM Standard D 1434. The test samples were prepared by compression molding at 165°C with a thickness around 300 μm.

Sample coding

The codes for the EPDM and nanocomposite samples are listed in Table III.

RESULTS AND DISCUSSION

Nanocomposite microstructure analysis

Figure 1 presents XRD spectra of neat organically modified montmorillonite (O-MMT) along with those of nanocomposite samples based on three different EPDM matrices composed of O-MMT and EPDM-*g*-MAH with a weight ratio of 5 : 5 (f_w = 1). The pristine O-MMT possesses three characteristic reflection peaks at 2θ values of 2.5, 4.5, and 7.2° corresponding to *d*-spacings of 3.4, 1.9, and 1.27 nm, respectively. The shift of the sharp d_{001}-plane spacing peak of O-MMT from 2θ = 2.5° to the lower diffraction angles in the three EPDM/EPDM-*g*-MAH/clay composites indicates that EPDM has been able to intercalate into the gallery spaces of the organoclay in the presence of EPDM-*g*-MAH as a compatibilizer, whereas no significant change has occurred in the absence of the compatibilizer (Fig. 2). However, the removal of the d_{001} spacing together with the lower peak density in the structure of the sample based on low-melt-viscosity EPDM (255) provides evidence of greater interdiffusion of the low-molecular-weight EPDM chains and therefore more intercalation of the silicate layers, which can lead to the enhanced delamination of the nanolayers.

It can also be observed in this figure that the nanocomposite sample based on the high-Mooney-viscosity and linear EPDM (755) exhibits a decrease in the d_{001} peak intensity compared with the 855 sample prepared by EPDM with a similar Mooney viscosity

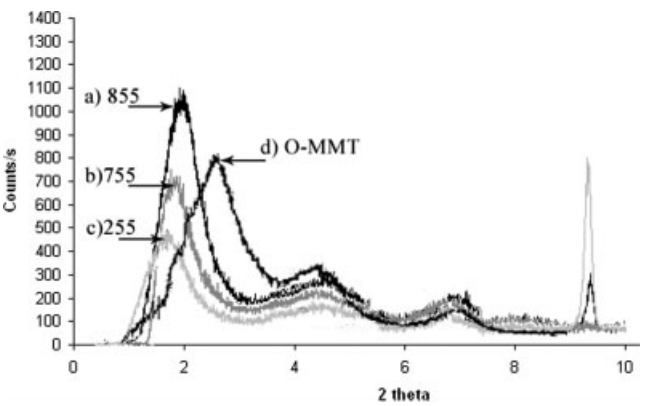

Figure 1 XRD patterns of (a) 855, (b) 755, (c) 255, and (d) O-MMT.

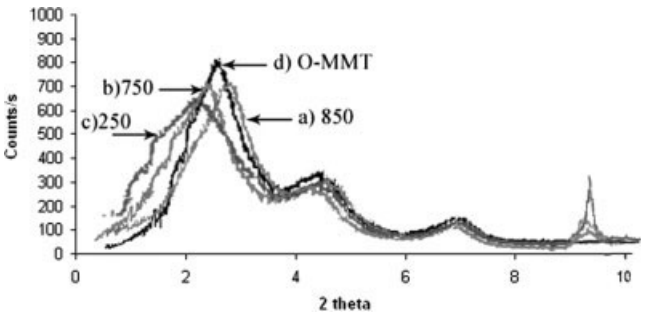

Figure 2 XRD patterns of (a) 850, (b) 750, (c) 250, and (d) O-MMT.

but with long-branch chains. This can be attributed to the steric hindrance effect of the branches, which retards the diffusion of the chains into the gallery spaces of the nanoclay, leading to the lower extent of interaction and therefore less delamination of the nanolayers.

However, it seems that in the melt compounding of nonpolar EPDM rubber and organomodified clay, the exfoliation of the clay platelets cannot be achieved at a high level unless there is sufficient compatibilization between the EPDM chains and clay layers. Therefore, similar nanocomposites were prepared with a higher EPDM-*g*-MAH to O-MMT ratio (f_w = 3) to assess the effectiveness of increased compatibilization on the foliation of clay nanolayers throughout the EPDM matrix. Figure 3 presents XRD patterns of the obtained hybrids. By comparing the micrographs in this figure with those given in Figure 1, we can clearly see that with the compatibilizer content increasing to 15 wt %, the two diffraction peaks that appear at $2\theta = 2.5^\circ$ and $2\theta = 4.5^\circ$ in the spectra of O-MMT have been removed in the XRD patterns of the two nanocomposites based on high-melt-viscosity EPDM rubber (7515 and 8515), regardless of the chain structural linearity. This indicates that the clay layers have been well dispersed as a result of high stress shearing of the layers during the melt compounding synergized with enhanced miscibility and interaction between the EPDM chains and clay platelets as a result of increased matrix polarity. The effectiveness of the polymer melt viscosity during the melt compounding of the nylon-6/nanoclay hybrids has also been reported.[3]

The XRD patterns of the nanocomposite sample based on low-Mooney-viscosity EPDM and 15 wt % EPDM-*g*-MAH (2515) exhibit the removal of the O-MMT characteristic peaks, a relatively small peak or shoulder within the low diffraction angles, and a gradual increase in the diffraction strength toward low angles. These results show that although increasing the polarity of low-molecular-weight EPDM facilitates the interdiffusion of the chains into the gallery spaces of the nanoclay, greater stress shearing of the clay nanolayers during the compounding of high-molecular-weight EPDM rubber with sufficient miscibility gives better delamination and dispersion of the nanolayers and thus enhanced interfacial interaction.

A better capacity for diffusion for low-molecular-weight polymers into the *d*-spacing of nanoclay has also been reported for rubber/clay hybrids.[1,18] Vaia and Giannelis,[21] using a thermodynamic model, have stated that there is a slight molecular weight dependence for melt intercalation that arises from an entropy change of the polymer. Other studies[19] show that the molecular weight affects only the intercalation kinetics, and the final microstructure is almost independent of the matrix molecular weight. It seems that the small chains diffuse more easily and quickly into the filler gallery spaces, whereas the high-molecular-weight matrices can produce more total shearing during mixing and, when good adhesion between the filler and matrix exists, lead to the breakage of the nanolayer stacking and increase their degree of exfoliation.

For all the nanocomposite samples, a narrow peak at $2\theta = 9^\circ$ is obvious and could be due to the generation of small crystals on the surface of the silicate layer.[16]

Tensile properties

A unique feature of polymer/clay nanocomposites is the remarkable improvement in their mechanical properties, such as the tensile strength and modulus. There are several parameters that can influence the properties of a polymer/clay nanocomposite, including the extent of interaction between the clay and polymer matrix, the state of dispersion, the nanofiller aspect ratio, and the microstructure. Attempts have been made to correlate the tensile modulus and strength of polymer matrices containing rigid particles, with each phase having an arbitrary modulus,

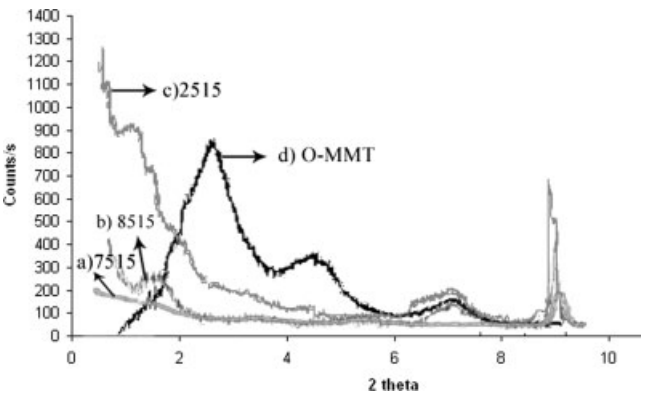

Figure 3 XRD patterns of (a) 7515, (b) 8515, (c) 2515, and (d) O-MMT.

TABLE IV
Tensile Properties of Various Samples

Property	Sample			
	200	250	255	2515
Tensile strength (kgf/cm^2)	16	27	46	47
Tensile modulus (kgf/cm^2)				
At 100% elongation	12	14	27	24
At 200% elongation	15	18	34	35
At 300% elongation	—	24	38	—
Elongation at break (%)	240	350	380	295
Measured L/d	—	5.5	939	618
	700	750	755	7515
Tensile strength (kgf/cm^2)	20	33	42	42
Tensile modulus (kgf/cm^2)				
At 100% elongation	13	16	26	24
At 200% elongation	14.5	21	32	34
At 300% elongation	20	30	38	—
Elongation at break (%)	300	315	305	265
Measured L/d		22	618	466
	800	850	855	8515
Tensile strength (kgf/cm^2)	21	34	31	53
Tensile modulus (kgf/cm^2)				
At 100% elongation	13	17	25	23
At 200% elongation	18	21	23	27
At 300% elongation	—	27	—	39
Elongation at break (%)	260	350	290	310
Measured L/d		47	529	386

to the filler shape and aspect ratio with classic mechanical models such as the Halpin–Tsai equation[22] or other equivalent equations.

According to the model, the shape and aspect ratio of the nanoparticle in the composite can be assessed by the modulus of the composite, as long as there is adhesion between the matrix and nanoparticle. In these equations, a coefficient named the Einstein constant (K_E) takes into account such factors as the filler geometry, packing geometry, loading conditions, and Poisson's ratio of the matrix. Therefore, the Einstein coefficient derived with the Halpin–Tsai equation modified by Lewis and Nilson[22] could represent the mean aspect ratio (L/d) of the dispersed particles. The generalized Halpin–Tsai expression for the shear, Young's, or bulk modulus of nanocomposites (M) is given next:

$$\frac{M}{M_{\text{Matrix}}} = \frac{1 + AB\phi_{\text{Clay}}}{1 - B\psi\phi_{\text{Clay}}} \tag{1}$$

where M_{Matrix} is the modulus of the matrix.

$$A = 1.33(L/d)^{0.645} \tag{2}$$

where constant A is equal to $K_E - 1$, ϕ_{Clay} is the volume fraction of the nanofiller, and constant B takes into account the relative modulus of the filler and matrix phase. It is defined as

$$B = \frac{M_{\text{Clay}}/M_{\text{Matrix}} - 1}{M_{\text{Clay}}/M_{\text{Matrix}} + A} \cong 1 \tag{3}$$

where M_{Clay} is the modulus of the clay.

The factor ψ depends on the maximum packing fraction (ϕ_m) of the filler (generally equal to 0.63) and can be expressed by the following relation:

$$\psi = 1 + \frac{1 - \varphi_m}{\varphi_m^2}\varphi_{\text{Clay}} \tag{4}$$

Therefore, the values of constant A in this work have been calculated with the measured tensile moduli of different nanocomposites, as presented in Table IV. The clay particles have been assumed to be randomly dispersed in three dimensions; thus, the modulus of the composite (M_{3DR}) can be calculated as follows:

$$M_{3DR} = \frac{1}{5}M_L + \frac{4}{5}M_T \tag{5}$$

where M_L and M_T represent the longitudinal and transverse moduli, respectively. In all calculations, constant A in the longitudinal direction has been estimated with eq. (2) and in the transverse direction has been assumed to have the value of 2.[23]

Figures 4 and 5 show stress–strain curves of the different prepared nanocomposite samples and vulcanized neat EPDM. The measured tensile properties of all the prepared samples are presented in Table IV. It can be clearly observed that the tensile strength and modulus of all the nanocomposites have been significantly enhanced both for high-molecular-weight and low-molecular-weight EPDM as a matrix by the addition of 5 wt % O-MMT. However, the degree of reinforcement is much more significant in the presence of EPDM-*g*-MAH as a

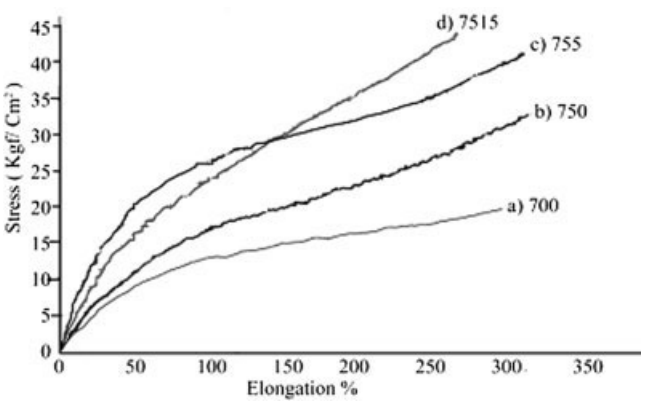

Figure 4 Tensile behavior of the nanocomposite samples based on linear high-molecular-weight EPDM and O-MMT (5 wt %): (a) neat EPDM (700), (b) composite without a compatibilizer (750), (c) EPDM/O-MMT composite (755) with 5 wt % EPDM-*g*-MAH as a compatibilizer, and (d) EPDM/O-MMT composite (7515) with 15 wt % compatibilizer.

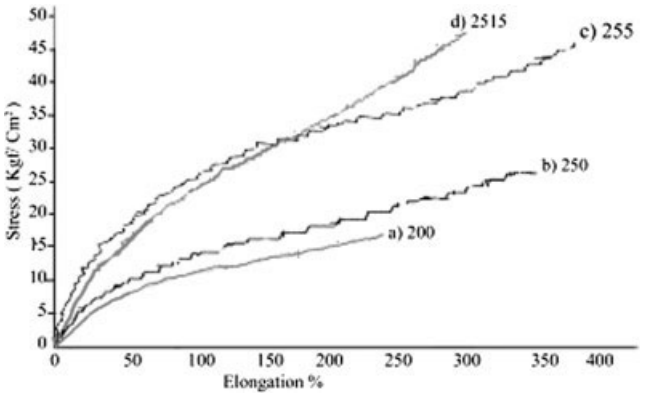

Figure 5 Tensile behavior of the nanocomposite samples based on branched low-molecular-weight EPDM and O-MMT (5 wt %): (a) neat EPDM (200), (b) composite without a compatibilizer (250), (c) EPDM/O-MMT composite (255) with 5 wt % EPDM-*g*-MAH as a compatibilizer, and (d) EPDM/O-MMT composite (2515) with 15 wt % compatibilizer.

compatibilizer. In both groups of nanocomposites, the samples with an EPDM-*g*-MAH/O-MMT ratio of 1 show lower tensile stress above 150% elongation than similar samples with an EPDM-*g*-MAH/O-MMT ratio of 3; nevertheless, the initial slope of the stress–strain curves corresponding to samples 255 and 755 is a little higher than that of samples 2515 and 7515. This might be attributed to the breakage of the flocculated structure of the nanolayers in the structure of the nanocomposites with 5 wt % EPDM-*g*-MAH. Greater flocculation and aspect ratios for the clay nanolayers have been measured for the less compatibilized nanocomposites, as shown in Table IV.

As the Halpin–Tsai model implies, the composite tensile modulus is expected to be more dependent on the filler aspect ratio, whereas the tensile strength is believed to be enhanced when a nanocomposite with a strong and defect-free interface is formed. The measured tensile properties for different EPDM/clay hybrids are in good agreement with this model. It can be concluded that nanocomposite samples containing a greater extent of nanolayer flocculation show a higher elastic modulus and stiffness than those with an intercalated and/or exfoliated structure. On the other hand, less flocculation of the clay platelets leads to a higher tensile strength. Moreover, the elongation at break for the interfacially compatibilized EPDM/O-MMT nanocomposites seems to be higher than that of unfilled crosslinked EPDM, and this indicates the reinforcement of the matrix by the dispersed nanolayers throughout the formed interfaces.

The EPDM/O-MMT samples having no compatibilizer (250,750, and 850) show insignificant reinforcement of the tensile properties, and the calculated L/d values for the nanolayers are smaller than the mean value of pristine O-MMT. On the other hand, the aspect ratio of the samples containing 15 wt % EPDM-*g*-MAH has been measured to be close to that of a single silicate layer (300–450 nm).[1] It is obvious from the data given in Table IV that the nanocomposite samples prepared with 5 wt % EPDM-*g*-MAH have a higher aspect ratio for the clay nanolayers, which is attributed to the greater flocculation tendency of the nanoclay platelets in these samples.

Dynamic melt rheology behavior

The melt linear viscoelastic behavior of the samples has been measured with the storage and loss modulus and is presented in Figure 6. All the EPDM nanocomposites exhibit a higher storage modulus within the low-frequency region in comparison with the neat EPDM, regardless of the EPDM type, and the modulus is higher for the samples with a clay/EPDM-*g*-MAH ratio of 3. This indicates the enhancement of the EPDM/clay interfacial interaction with the increasing polarity of the EPDM matrix. EPDM-*g*-MAH is expected to play a dual role as it can improve the dispersion of the nanoclay layers and lead to an increase in the degree of polymer–filler interfacial interaction throughout the matrix.

At high frequencies, the moduli of the nanocomposite samples reaches those of neat EPDMs. This can be explained by the fact that at low frequencies the time is long enough to unravel the chain entanglements within the structure of the neat EPDMs; thus, a large amount of relaxation occurs and results in a low modulus. Meanwhile, when the frequency is so high that the chain cannot relax sufficiently in the presence of entanglements, the modulus will increase. Nevertheless, in composite samples, the dispersed nanolayers decrease the extent of chain entanglements in the amorphous zones,[24] leading to a lower dependence of the nanocomposite modulus on the frequency and a lower increase in the modulus within the high-frequency regions in comparison with the neat EPDM.

However, all the nanocomposites exhibit a lower rate of increase in the storage modulus within the low-frequency region than the pristine EPDMs. Samples 7515 and 8515 show less frequency dependence than 2515, and this is consistent with the XRD patterns measured for these samples, as more flocculation occurs by the clay nanolayers in the low-Mooney-viscosity EPDM matrix.

According to the classical theory of a suspension's rheology for conventional composites,[20] the rotation of filler particles in a matrix, as a source of relaxation, is possible only when the filler volume fraction is less than the inverse of the filler aspect ratio [$(L/d)^{-1}$]. Thus, in flocculated nanocomposite samples

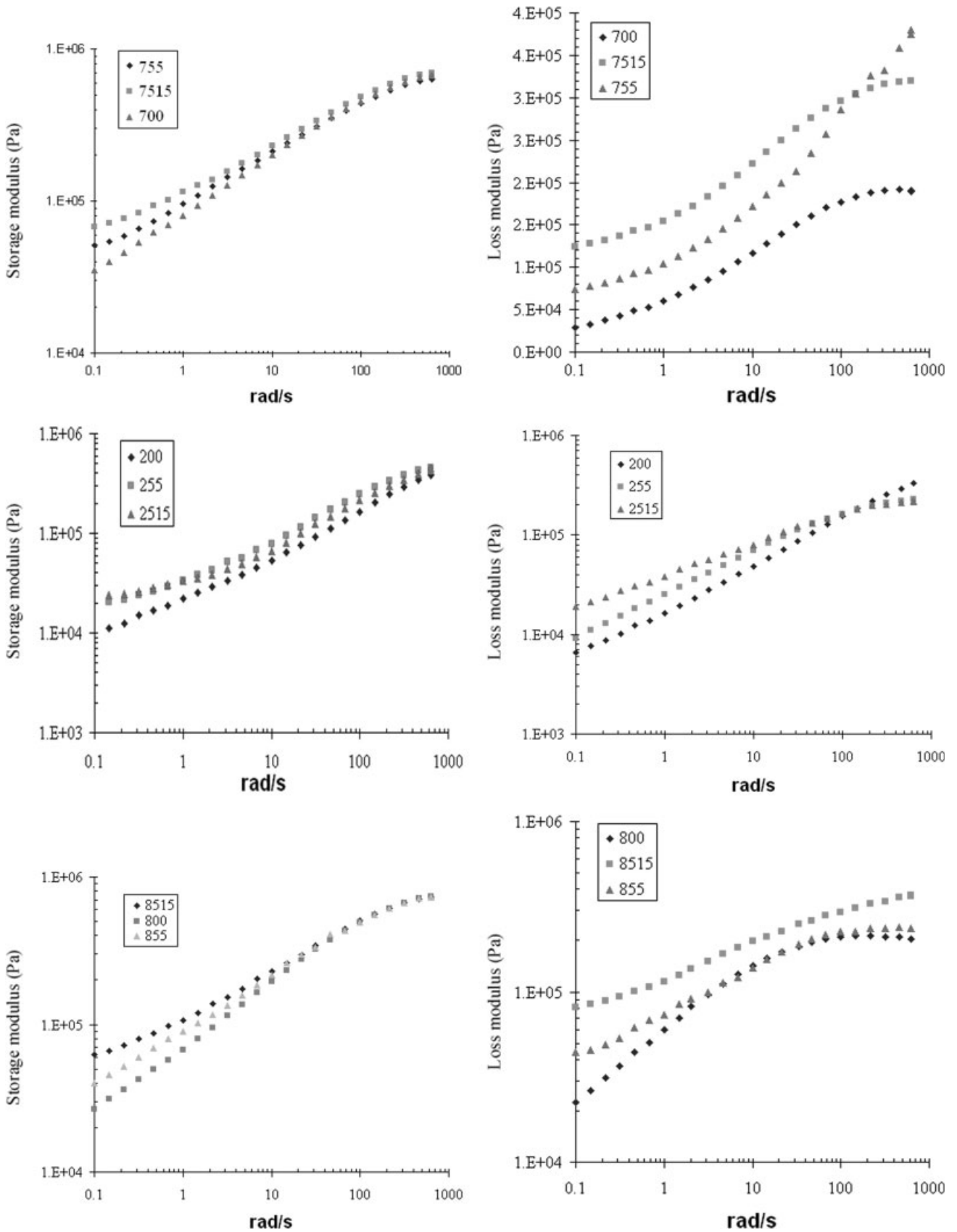

Figure 6 Comparison of the linear viscoelastic behaviors of EPDM/O-MMT hybrids based on different EPDM grades.

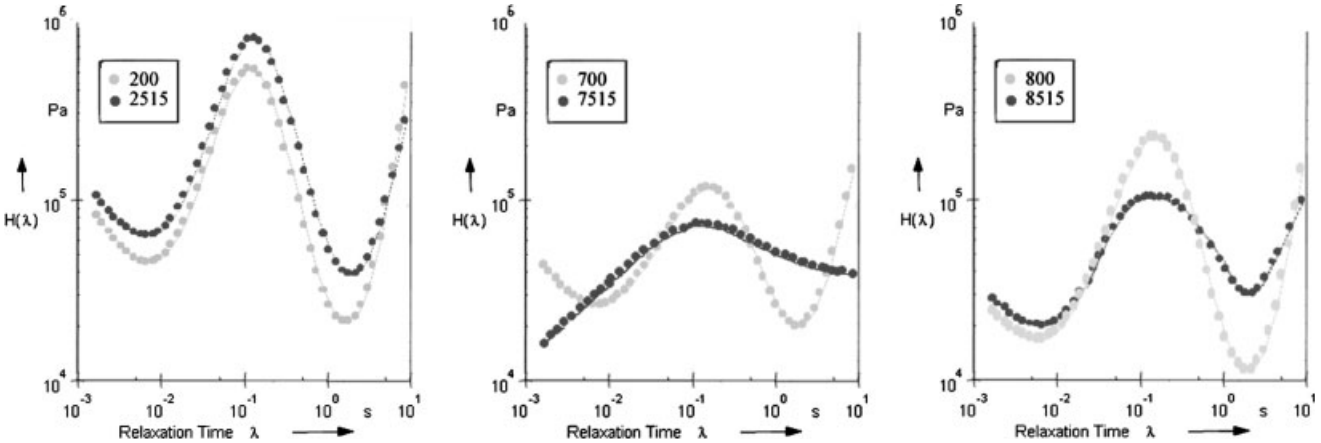

Figure 7 Retardation time function of the nanocomposite samples.

such as 255, 2515, 755, and 855, the rotation of the laterally stacked silicate layers might be hindered $[(L/d)^{-1}$ is ca. 0.03–0.016], and only translational motion is possible; therefore, a higher modulus is shown. Nonterminal behavior has been also explained by the long-range domain structure, topological defects, and molecular relaxation retardation.[1,20,25]

In Figure 7, the relaxation time distribution functions for the nanocomposites based on EPDM grades with different structural features are presented and compared with those of the corresponding neat EPDM. Both high-Mooney-viscosity-based samples show a wider distribution spectrum for the relaxation times than the sample prepared with the low-Mooney-viscosity EPDM (2515). This is in agreement with the XRD patterns obtained for these samples. Sample 7515 shows a much wider distribution, and this indicates a better distribution of the clay nanolayers, which leads to greater hindrance of the chain segmental motions.

Oxygen permeability and solvent absorption

The incorporation of layered structure nanofillers into polymer matrices has been shown to be highly effective in reducing gas and solvent permeability.[20,22] This has been attributed to the formation of a torturous path by the dispersed nanolayers. In Table V, the oxygen gas permeability for different prepared EPDM/O-MMT composites on low-molecular-weight and high-molecular-weight EPDM rubber with different chain linearities is presented. The presence of silicate layers in the EPDM matrix has led to a decrease in the O_2 permeability. However, all the composite samples prepared by the high-Mooney-viscosity EPDM (code 7) show lower permeability, even with a low interfacial compatibilizer content. The best barrier property is shown by sample 7515, which contains 15 wt % EPDM-*g*-MAH as a compatibilizer. This is consistent with the observed microstructure for sample 7515, as the clay nanolayers have been dispersed to a greater extent as a result of high shearing imposed on the clay nanolayers during mixing.

According to the Nilson model,[22] the dispersion of clay plates in a parallel form in a polymer matrix produces a maze with a tortuosity factor (τ) that can be expressed by the following equation:

$$\tau = \frac{d'}{d} = 1 + (L/2d)\,\phi_{\text{Clay}} \tag{6}$$

where ϕ_{Clay} is the volume fraction of the dispersed particles. Therefore, the relative permeability coefficient can be calculated with

$$\frac{P_{\text{nanocomposite}}}{P_{\text{EPDM}}} \frac{1}{1 + (L/2d)\phi} \tag{7}$$

where P_{EPDM} and $P_{\text{nanocomposite}}$ are the permeation coefficients of neat EPDM and nanocomposite samples containing 5 wt % O-MMT, respectively.

According to this equation, the gas permeability of composites must be related only to the volume fraction and aspect ratio of the clay particles. However, the permeation of samples with a flocculated microstructure, which possess much higher aspect ratios, is a little lower than that of samples with better clay dispersion (samples 2515 and 7515). In nanocomposite samples, the extent of exfoliation should also be taken into account. In classic composite models, the

TABLE V
O_2 Gas Permeation Coefficient of Neat EPDMs and Different EPDM/O-MMT Composites

Sample	200	255	2515	700	755	7515
Permeation (cm^3/m^2 day bar)	630	580	510	585	461	315

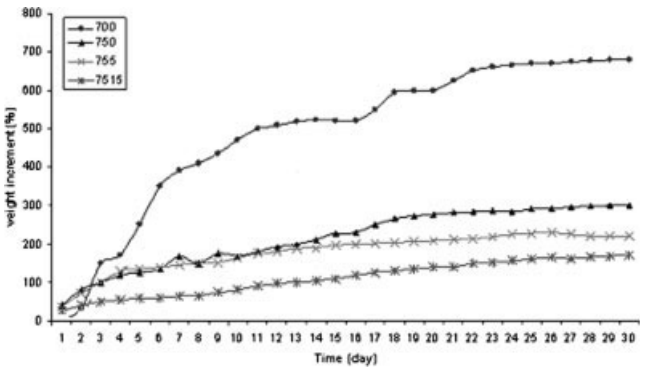

Figure 8 Solvent absorption of various samples immersed in pure hexadecane at room temperature.

fraction of stacked fillers is negligible, so the volume fraction of the filler is a good measure for calculating the path of permeating molecules. Moreover, the number of separated particles and their aspect ratio as well as the silicate layer orientation in the matrix are important in calculating the tortuosity factor for a nanocomposite. In flocculated systems, when the silicate layers stack laterally together, the aspect ratio increases significantly. However, in EPDM/O-MMT samples, the silicate layers tend to stack in all directions, and the thickness of the clay particles also increases at the same time. Therefore, there will sometimes be many silicate layers in a flocculated–intercalated state with a higher aspect ratio than those of separate dispersed nanolayers.

The solvent absorption of the vulcanized samples has been evaluated with hexadecane, which is a good solvent for EPDM at room temperature. The results are presented in Figure 8. The solvent absorption of composite 7515 is about one-fourth of that of sample 700. In addition, all initial adsorption rates of the nanocomposite samples have decreased nearly to one-third of that of the neat pristine EPDM. These phenomena could be also attributed to the formation of a torturous path by the silicate nanolayers.

TGA

The nonisothermal weight-loss curves obtained through TGA for different EPDM/O-MMT composites are presented in Figure 9. Neat EPDM (sample 700) has a very sharp weight loss between 375 and 425°C followed by a short step near 500°C. However, the nanocomposite samples show a small, gradual weight loss above 200°C with a higher degradation temperature, and this indicates the improved thermal resistance of the EPDM/O-MMT nanocomposites. The better thermal resistance is obvious for the interfacially compatibilized samples (7515 and 755) and is the result of more and better dispersion of the clay nanolayers. This leads to the conclusion that the incorporation of EPDM-*g*-MAH into the structure of the EPDM/nanoclay composites can be beneficial in improving the thermal resistance of the samples.

The first gradual loss might be due to thermal degradation of the ammonium salt inside the filler or the evaporation of its humidity. Sample 750, a noncompatibilized EPDM/O-MMT hybrid, degrades at a temperature about 20°C lower than that of the other nanocomposites because of poor dispersion of O-MMT in the matrix in this sample. In nanocomposite samples, the degradation rate (the slope of the weight-loss curve) is about half that of neat EPDM, and the major degradation temperature is improved about 40°C.

This improvement in the thermal stability can be attributed to the presence of impenetrable silicate layers with a large aspect ratio, offering a great barrier effect to hinder the migration of small molecules (resulting from thermal decomposition) to the surface. These layers could also reduce the heat flow in the samples.[13] Sirivastaka et al.[26] also believe that the coexistence of intercalated and exfoliated silicate layers in an EPDM matrix, which increases the Si—O—C interfacial interaction to restrict the thermal motion of EPDM polymer segments, is another possibility

CONCLUSIONS

EPDM/O-MMT nanocomposites have been successfully prepared by melt compounding with EPDM-*g*-MAH as an interfacial compatibilizer. XRD analysis indicates that matrix chains can be intercalated into the gallery space of O-MMT effectively. Moreover, the outstanding improvement in the nanocomposite properties confirms that silicate layers of the organoclay have been dispersed on a nanometer scale in the EPDM matrix.

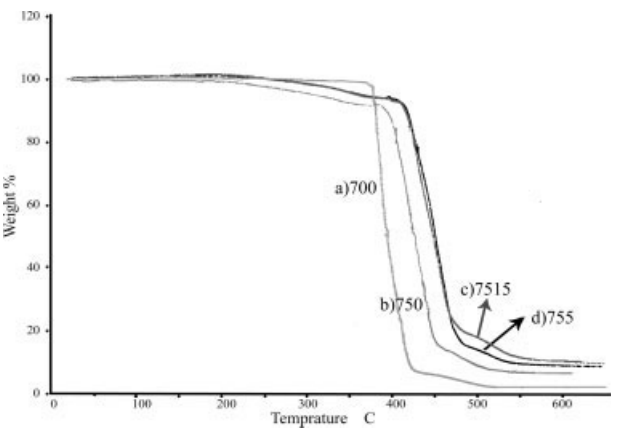

Figure 9 TGA results for neat EPDM and different nanocomposite samples.

An almost complete dispersion was obtained when the compatibilizer–filler ratio was 3. In the samples containing less EPDM-*g*-MAH, strong flocculation of the stacked dispersed clay particles was evidenced.

Better dispersion of the silicate layers can be obtained in EPDM matrices with a higher Mooney viscosity, as they exert higher shearing during mixing. Also, the linear polymer chains can be more intercalated into O-MMT galleries than long-branch EPDM chains.

The higher extent of silicate layer dispersion leads to greater improvements in the properties of nanocomposites, such as the tensile modulus, swelling, thermal resistance, and gas-barrier properties.

The enhancement of the storage modulus (in the melted state) and decrease in the terminal slope, as well as the broadening of the retardation time spectra, for the nanocomposites containing more compatibilizer indicate strong interactions between the O-MMT and EPDM matrix in the molten state.

The dispersion of impermeable O-MMT with a planar orientation in nanocomposite samples leads to improved solvent and thermal resistance and gas-barrier properties.

References

1. Ray, S. S.; Okamoto, M. Prog Polym Sci 2003, 28, 1539.
2. Ahmadi, S. J.; Huang, Y.; Li, W. Compos Sci Technol 2005, 65, 1069.
3. Fornes, T. D.; Yoon, P. J.; Keskkula, H.; Paul, D. R. Polymer 2001, 42, 9929.
4. Zheng, H.; Zhang, Y.; Peng, Z.; Zhang, Y. Polym Test 2004, 23, 217.
5. Ganter, M.; Gronski, W.; Semke, H.; Zilg, T.; Thomann, C.; Muhlhaupt, R. Kautsch Gummi Kunstst 2001, 54, 166.
6. Mousa, A.; Karger, K. J. Macromol Mater Eng 2001, 286, 260.
7. Yen, T. V.; James, E.; Mark, L. H.; Pham, M. E. J Appl Polym Sci 2001, 82, 1391.
8. Okada, A.; Usuki, A.; Kurauchi, O. In Hybrid Organic–Inorganic Composites; Mark, J. E.; Lee, C. Y. C.; Branconi, P. A., Eds.; ACS Symposium Series; American Chemical Society: Washington, DC, 1995.
9. Young, W. C.; Yungchul, Y.; Kato, M. Polymer 2002, 43, 2185.
10. Peter, C.; Lebaron, N.; Thomas, J.; Pinnavaia, T. J. Chem Mater 2001, 13, 3760.
11. Markus, G.; Wolfarm, G.; Peter, R.; Rolf, M. Rubber Chem Technol 2001, 74, 221.
12. Wang, Y. Z.; Zhang, L. Q.; Tang, C. H. J Appl Polym Sci 2000, 78, 1879.
13. Parija, S.; Nayak, S. K.; Verma, S. K.; Tripathy, S. S. Polym Compos 2004, 25, 646.
14. Nguyen, Q. T.; Baird, D. G. Adv Polym Technol 2006, 25, 270.
15. Kim, D. H.; Park, J. U.; Cho, K. S.; Ahn, K. H.; Lee, S. J. Macromol Mater Eng 2006, 291, 1127.
16. Ma, Y.; Wu, Y.-P.; Wang, Y.-Q.; Zhang, L.-Q. J Appl Polym Sci 2006, 99, 914.
17. Liu, B.-L.; Ding, Q.; He, Q.-H.; Cai, J.; Hu, B.-X.; Shen, J. J Appl Polym Sci 2006 99, 2578.
18. Li, W.; Huang, Y. D.; Ahmadi, S. J. J Appl Polym Sci 2004, 94, 440.
19. Vaia, R. A.; Jandt, K. D.; Kramer, E. J.; Giannelis, E. P. Macromolecules 1995, 28, 8080.
20. Ray, S. S.; Okamoto, K.; Okamoto, M. Macromolecules 2003, 36, 2355.
21. Vaia, R. A.; Giannelis, E. P. Macromolecules 1997, 30, 8000.
22. Nilson, L. E.; Landel, R. F. Mechanical Properties of Polymers and Composites, 2nd ed.; Marcel Dekker: New York, 1994.
23. Agarwal, B. D.; Broutman, L. J. Analysis and Performance of Fiber Composites; Wiley-Interscience: New York, 1980.
24. Mishra, J. K.; Hwang, K.-J.; Ha, C. S. Polymer 2005, 46, 1995.
25. Krishnamoorti, R.; Giannelis, E. P. Macromolecules 1997, 30, 4097.
26. Acharya, H.; Pramanik, M.; Srivastava, S. K.; Bhowmick, A. K. J Appl Polym Sci 2004, 93, 2429.